IEEE Photonics Journal
An IEEE Photonics Society Publication

Open Access

A Multimetal Broadband Metamaterial Perfect Absorber With Compact Dimension

Volume 8, Number 2, April 2016

Yan Kai Zhong
Sze Ming Fu
Ming-Hsiang Tu
Bo-Ruei Chen
Albert Lin

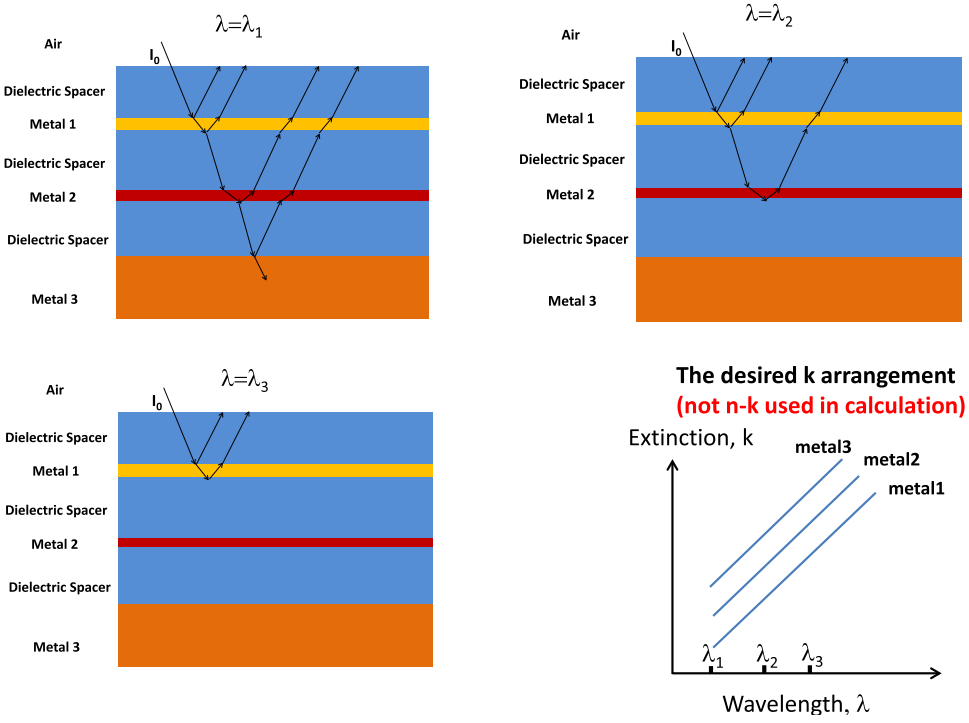

DOI: 10.1109/JPHOT.2016.2543003
1943-0655

A Multimetal Broadband Metamaterial Perfect Absorber With Compact Dimension

Yan Kai Zhong, Sze Ming Fu, Ming-Hsiang Tu, Bo-Ruei Chen, and Albert Lin

Department of Electronic Engineering, National Chiao-Tung University, Hsinchu 30010, Taiwan

DOI: 10.1109/JPHOT.2016.2543003

Manuscript received February 11, 2016; revised March 10, 2016; accepted March 14, 2016. Date of publication March 23, 2016; date of current version March 30, 2016. Corresponding author: A. Lin (e-mail: hdtd5746@gmail.com).

Abstract: We propose an extremely simple multiple-metal metamaterial perfect absorber (MPA). The dimension of our proposed design is only 221 nm for the visible wavelength range from 400 to 700 nm. This is comparable with past efforts on MPAs using plasmonics at the same wavelength range, whereas the plasmonic excitation is absent in our proposal. A unity broadband absorption can be achieved with ultrathin metallic films. In addition, the wavelength scalability is possible using our design, and the fully planar simple configuration facilitates large-area photonic design without the need for lithography and etching. The physics is the field penetration and the field absorption for the photons at different wavelength ranges using different metallic layers. We also show that the adjustment of the individual layer thickness is critical to attaining a perfect wave impedance matching to vacuum. The titanium (Ti), nickel (Ni), and aluminum (Al) triple-metal configuration is used to demonstrate the concept experimentally, and a close match to the theoretical result is observed. The absorption band can be further widened with more stacking layers with various metals. We believe that the proposed design is very promising in the aspects of simple processing and scalable for large-area broadband unity absorption. It thus improves the future implementation of MPAs and facilitates a wide range of relevant applications.

Index Terms: Photonic materials, metamaterials, photonic materials and engineered photonic structures.

1. Introduction

Perfect absorption has been an emerging research field over the past few years due to its broad applications in the fields of biomedical optics [1], [2], ultra-high sensitivity sensing [3], antenna systems [4], cloaking [5], radar cross section (RCS) reduction [6], thermal emitter [7], and thermophotovoltaic (TPV) [8]. The photonic device of this kind is termed metamaterial perfect absorbers (MPA). The unity absorption can be of narrowband or broadband nature, and depending on the applications, either narrow or broadband response is desired. From optics point of view, narrow band unity absorption is easier to achieve. Several different physical phenomena can provide very high absorption at a specific wavelength such as quasi-guided mode excitations or Fabry-Perot resonances. These phenomena can thus be utilized to achieve narrowband MPA designs. On the other hand, a broader bandwidth MPA requires special

consideration, and implementing such devices is not simple. This is due to the fact that quasi-guided modes or guided resonances cannot exist over the entire broad wavelength range, and this prevents the use of conventional diffractive optics methodology to realize broadband MPAs.

The past effort on broadband metamaterial perfect absorbers has been developed using plasmonic resonant structures [3], [9]–[11]; patterned metallic grating on dielectric [1], [3], [11]–[14]; metal-dielectric-metal with nanostructures [1], [9]; and adiabatic light coupling using hyperbolic metamaterials nanotips [15]–[17]. The plasmonic structures, in general, utilize the plasmonic mode excitations in silver or gold nanostructures. Under this scenario, strong field intensity inside the metallic material leads to an enhanced absorption. Although, in photovoltaics, the metal absorption is a waste, in many other photonics applications, this is the desired power dissipation including high sensitivity sensors and thermophotovoltaics (TPV) emitter-absorber. The advantage of using plasmonic modes is that the photonic device dimension can be made more compact than traditional optical nanostructures based on diffractions and light scattering. The first miniaturized plasmonic ultrabroadband perfect absorber is revealed by the work of Atwater *et al.* [9], the compact dimension achieved is 260 nm for the visible (VIS) wavelength range from 400 nm to 700 nm. This is due to the condensed field intensity associated with the surface plasmon polariton (SPP) and localized surface plasmon (LSP). The slight limitation on plasmonic absorber is that the wavelength scalability is less possible due to the plasmonic mode wavelength is largely determined by the material dispersion. Additionally, the plasmonic mode excitation over an ultrabroad bandwidth can be more difficult to achieve. This makes that the plasmonic absorbers may be more suitable for a moderate bandwidth application.

On the other hand, the proposal of the ultra-long tapered hyperbolic metamaterial (HMM) broadband absorbers by Fang *et al.* [16] provides extremely wide absorption band that is never achieved before. The physics is that the adiabatic coupling achieved with the tapered-sidewall photonic nanostructures is robust over a very broad spectral range. The hyperbolic dispersion of the metal-dielectric stacking further enhance the light absorption by the unbounded photonic density of states (PDOS). In this scenario, the incident photons are coupled into the metallic films from the side of the HMM nano-tips or nanocones, and the photons of different wavelengths will be absorbed by different portions of the HMM stacking as illustrated in the literature [16]. The slight limitation of HMM nanotips can be the scalability to large-area fabrication and the ultra-long dimension compared to the plasmonic absorbers. The ultra-long dimension with tapered nanostructures can lead to process difficulty using regular lithography and etching techniques.

In this work, we proposed a very simple planar multiple-metal configuration for metamaterial perfect absorbers. The structure has the advantage that the device thickness is only 221 nm for the metamaterial perfect absorbers at visible wavelength range from 400 nm to 700 nm. This is comparable to the plasmonic metamaterial perfect absorbers [9] at the same wavelength range. As a result, our design using field penetration facilitates the miniaturization of the nano-photonic devices similar to plasmonics. Additionally, the absorbance that can be achieved is close to unity, similar to tapered HMM absorbers. The physics and design of this proposed multi-metal structure are based on the different extinction coefficients (k) for different metallic materials. The sequential arrangement of the metals from the lowest to the highest extinction coefficient can lead to very efficient absorption over the desired frequency ranges. This is not surprising since an absorbing material with a moderate k value is the most suitable for perfect absorbers using field penetration. Excessively large k value leads to reflections, while insufficient k value leads to low absorption. While most metallic materials in practice have strong dispersion in wavelength, choosing a single metal for a broadband absorption can be very challenging unless an elaborate and complex design such as HMM is established. Therefore, using multiple metals can be advantageous in this aspect, and assigning the absorption bands at different wavelength ranges to different metallic materials for a full absorption is one way to overcome the above-mentioned k-value dispersion problem.

In addition to the multiple-metal configurations, the dielectric spacer, which is silicon dioxide (SiO_2) in our case, is also important to achieve the impedance matched condition for the

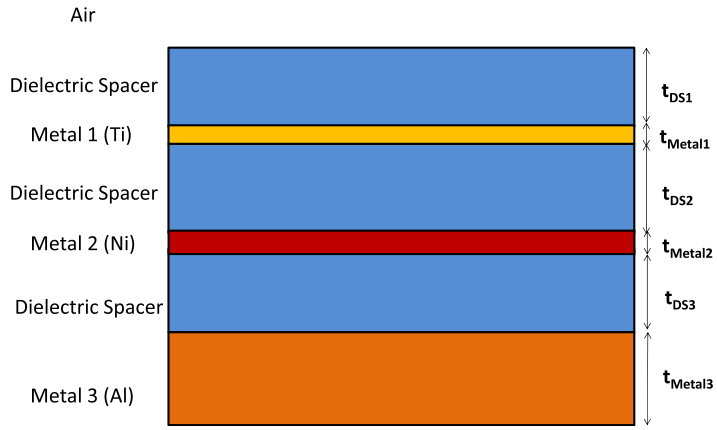

Fig. 1. Multiple-metal multi-junction type metamaterial perfect absorber. In this work, metal 1 is selected as titanium (Ti), metal 2 is selected as nickel (Ni), metal 3 is selected as aluminum (Al), and the dielectric spacer is silicon dioxide (SiO_2). Other metals or dielectrics can also be used, and more than 3-metal stacking is likely to further enhance the bandwidth if desired.

incident photons. We analyze the wave impedance for the perfect absorber stack with varied thickness of the SiO_2 and the metallic layers. Since the proposed structure is fully planarized, it does not require any lithography and etching and, therefore, totally scalable to large-area processing such as TPV emitter-absorber. The wavelength scalability is also demonstrated in this work, and it is feasible to use the proposed multi-metal design in photonic applications of a wide frequency range.

2. Multi-Metal, Compact Metamaterial Perfect Absorbers

In this work, we use rigorously coupled wave analysis (RCWA) in Rsoft DiffractMod [18]. While the RCWA can be used to analyze grating in two or three dimensions, it can also be used to calculate planar structures with full accuracy. The eigenmode expansion is implemented in this software, and the series expansion is utilized to represent the optical fields. The material parameters are measured using a J. A. Woollam M2000 ellipsometer for aluminum (Al), titanium (Ti), nickel (Ni), SiO_2. The calculation is conducted using Intel Xeon 3.1 GHz Quadcore CPU. Since the proposed design is a planar multilayer structure, the computation is very fast even with the iterative optimization of the layer thickness using a genetic algorithm (GA). The genetic algorithm is a global optimization technique that uses the flow of nature adaptation to tackle difficult convergence optimization problems. For conventional optimization algorithms such as Newton's method, the slope of the objective function has to be known in order to gradually approach the local maximum. In this case, the objective function has to be smooth and differentiable. Nevertheless, for many optimization problems, the objective function is not differentiable, or its derivatives cannot be expressed analytically. Thus, the global optimization algorithm becomes important and more versatile in this scenario. It is also worth a mention that genetic algorithm (GA) is among the most effective global optimization algorithm [19]–[25]. It requires no initial guess, requires no derivatives, and can locate a local or even global maximum for ill-behaved non-smooth objective functions. For the case of nano-photonic perfect absorbers, the complex field penetration and absorption can lead to a very large and irregular searching space and, therefore, we choose GA to locate the proper geometry for the study below.

Fig. 1 illustrates the proposed multi-metal structures for metamaterial perfect absorbers. The sequential arrangement of the metals is very critical. Normally the high extinction metal should be placed at the bottom since the field penetration is unlikely for the high extinction metal. Placing high extinction metal on the top prevents further absorption by the metallic layers below. As illustrated in Fig. 2(a)–(c), the ray traced analysis reveals multi-junction configuration and the cancelation of the reflected wave. Fig. 2(d) plots the illustration of typical metal *k*-value

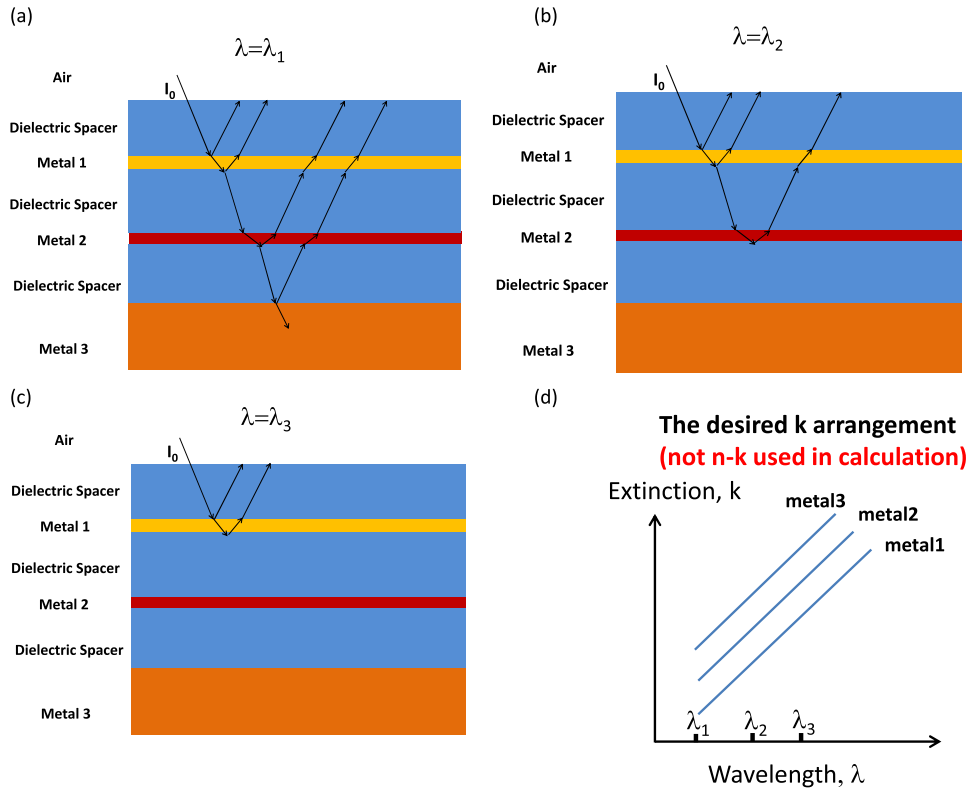

Fig. 2. Design principle for the multi-junction type metamaterial perfect absorbers. The photons with different energies are dissipated in different parts of the metamaterial perfect absorber (MPA). This is accomplished by using carefully arranged metal combination with varying extinction. The dimension can be comparable to plasmonic-based design due to field penetration. (d) Desired extinction coefficient arrangement: sequentially increased extinction (k) for various metals. The actual $n-k$ used in calculation is shown in Fig. 3.

dispersion. For most metals, the k-value, in general, increases with wavelength for the wavelength range from visible to near infrared. For the short wavelength range (λ_1), since the absorption coefficient or the k-value is still low for metal 1 and metal 2, incident field penetrates metal 1 and metal 2 and reaches the high extinction metal 3 at the bottom. For middle wavelength range (λ_2), the extinction coefficient k-value for metal 2 becomes high enough for full absorption. This is due to the dispersion of typical metals as illustrated in Fig. 2(d). In this case, the penetration through metal 2 is unlikely, and the field will be dissipated in metal 1 and metal 2. For long wavelength range (λ_3), the k-value of the metal 1 now becomes high enough, and the field absorption will greatly happen at metal 1. The field plots for different wavelengths will be given below, and it will be clear that the description in this paragraph is indeed the physics that happens in the multi-metal perfect absorbers.

Fig. 3 shows the material $n-k$ for Al, Ni, and Ti. Fig. 3(b) shows nice agreement with the desired k-values in Fig. 2(d). The desired k-value arrangement is shown in Fig. 2(d), where three metals with high, medium, and low k-values are used. Among the selected real materials, Al has the highest extinction, and its extinction coefficient begins to rise at short wavelength range. Therefore, Al should certainly be placed at the bottom. Notice that at $\lambda = 190$ nm–668 nm, Ti and Ni have quite close k-value. For other wavelength ranges, $k_{Al} > k_{Ni} > k_{Ti}$ persists. It is worth mention that $k_{Al} > k_{Ni} > k_{Ti}$ prevails for wavelength beyond $\lambda = 1680$ nm, the upper wavelength limit of our ellipsometer. This point can be verified in many optical constant databases [26]. For the MPAs in Fig. 4 below, there is no doubt that Ti/Ni/Al arrangement should be used for Fig. 4(b) ($\lambda = 580$ nm–1050 nm) and Fig. 4(c) ($\lambda = 900$ nm–1670 nm). For Fig. 4(a) ($\lambda = 400$ nm–700 nm), Ti/Ni/Al or Ni/Ti/Al can be used. The similar k-value for Ti and Ni in the

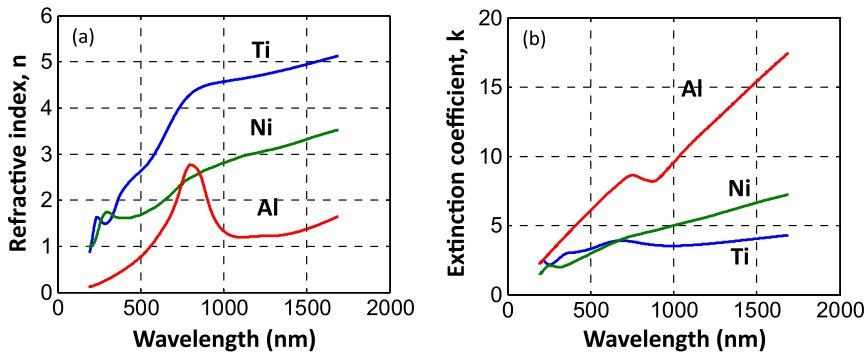

Fig. 3. Material properties of the metals in this study. The measurement is done using a. J. A. Woollam M2000 ellipsometer. (a) Refractive index (n). (b) Extinction coefficient (k). This is the $n-k$ values used in calculation.

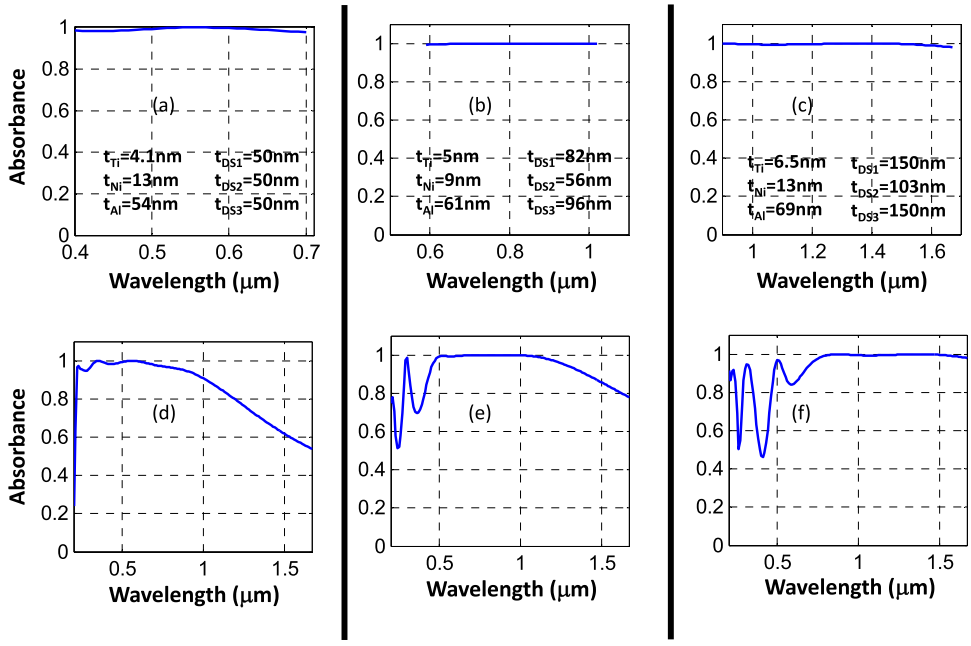

Fig. 4. Calculated broadband absorption for multi-metal configurations. (a)–(c) Wavelength range for genetic algorithm (GA) optimization. (a) $\lambda = 400$ nm–700 nm for visible metamaterial perfect absorbers. (b) $\lambda = 580$ nm–1050 nm for near-infrared (NIR) metamaterial perfect absorbers. (c) $\lambda = 900$ nm–1670 nm for near-infrared (NIR) metamaterial perfect absorbers. (d)–(f) Corresponding full spectral absorption spectrum from $\lambda = 200$ nm–1670 nm for (a)–(c). Wave-range is selected according to the ellipsometer-measured $n-k$ wavelength range in our lab. This is a typical $n-k$ measurement range for ellipsometry. Longer wavelength $n-k$ deep into IR requires special equipment. For the (a) and (d) part, the total thickness is 221 nm, which is comparable to the plasmonic metamaterial perfect absorber [9].

wavelength regime in Fig. 4(a) makes both configurations feasible. In addition, the adjustment in Ti and Ni film thickness can effectively compensate and correct the *k*-value deviation from the desired one. For consistency, we uniformly choose the Ti/Ni/Al configuration for all MPAs in Fig. 4. It is worth to say that the Ti/Ni/Al configuration is also suitable for the wavelength beyond $\lambda = 1680$ nm. For the stacking of more than three metallic materials, a wider absorption band can result. The design principles and the methodologies are the same as the three metals metamaterial perfect absorbers presented in this work.

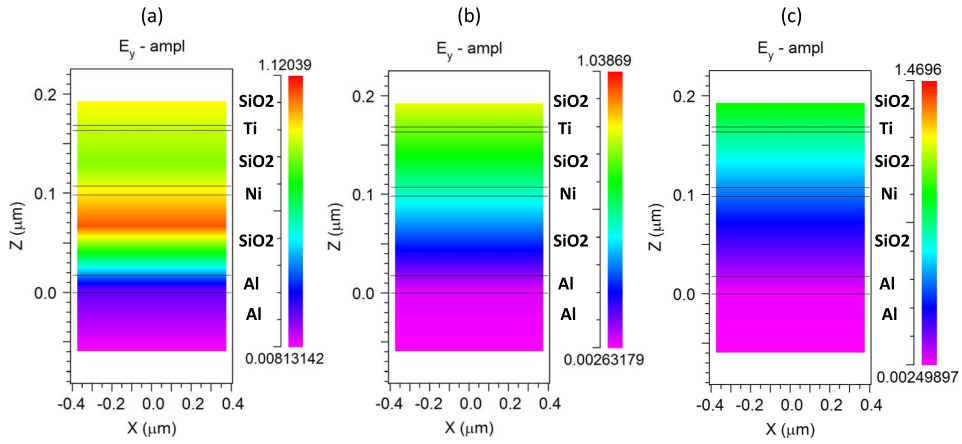

Fig. 5. Time-harmonic steady state electric field profile E_y for (a) $\lambda = 0.3$ μm, (b) $\lambda = 0.8$ μm, and (c) $\lambda = 1.67$ μm. The dimension is $t_{\text{Ti}} = 5$ nm, $t_{\text{Ni}} = 9$ nm, $t_{\text{Al}} = 61$ nm, $t_{\text{Ds1}} = 82$ nm, $t_{\text{DS2}} = 52$ nm, and $t_{\text{DS3}} = 96$ nm, corresponding to Fig. 4(b). In fact, the physics in Fig. 4(a)–(c) are all the same. Fig. 4(b) is used to illustrate the sequential absorption due to the range of the ellipsometer, which is from $\lambda = 0.2$ μm to $\lambda = 1.68$ μm. Therefore, in Fig. 4(b), it is the easiest to demonstrate the successive absorption at different wavelength ranges. In order to demonstrate the same phenomenon for Fig. 4(a) or (c), $n - k$ data beyond 1.68 μm or below 0.2 μm is necessary.

3. Theoretical Result

The simulation is conducted using the RCWA algorithm. Although scattering matrix method can also be used, it is undoubtedly that RCWA can also provide a very accurate result. In fact, the RCWA with diffraction order of zero is equivalent to scattering matrix method for a planar structure. The GA is effective to locate the optimal geometry for this multi-metal structure for metamaterial perfect absorbers. The film thickness is critical for field penetration, which is the key part in multi-junction configurations since photons with different energies are going to be absorbed by different sub-cells. If the thin film thickness becomes too thick, the bottom cells are invisible for incoming photons. For the film thickness that is too thin, insufficient absorption occurs, and this results in imperfect metamaterial perfect absorbers. Another important feature of this proposed design is that it does not count on plasmonic effect. This is because the design is a planar structure and, therefore, plasmonic mode excitation is absent. This fact improves the wavelength scalability of the design. Fig. 4 shows that the multi-junction metamaterial perfect absorbers can be used not only for visible wavelength range. The corresponding film thicknesses are also shown in Fig. 4. With some adjustment in the film thickness, the broadband absorption can be shifted toward infrared. This flexible adjustment in absorption band is more difficult to achieve if plasmonic resonance is used to boost the absorption. This is due to the fact that for plasmonic mode excitations, the wavelength of the excitations is fixed largely by the material properties. Although adjusting the geometry and using grating coupling can shift the plasmonic resonance wavelengths, the shifting range in wavelength is limited and not arbitrary.

Fig. 5 shows the field profiles for the multiple metal multi-junction metamaterial perfect absorbers. It is clear that for short wavelength photons, the penetration is all the way through the thin film stacks and reaches the aluminum layer at the bottom. For the mid wavelength, the photons are stopped at the Ni layer, and the full absorption is achieved in a large part by the extinction of the Ni. The Ti layer, in this case, is not highly-extinct enough to fully absorb the mid-wavelength range photons. For long wavelength photons, the Ti extinction becomes high enough at long wavelength range, and it is clear that at this wavelength range, photons are absorbed fully by the Ti layer. The field is therefore not penetrating into Al or even Ni layer. Due to the design of multiple metals, the absorption at broadband can be achieved by allocating different wavelength ranges in the spectrum to different metallic materials. Fig. 6 plots the angular responses for the visible (VIS) metamaterial perfect absorber in

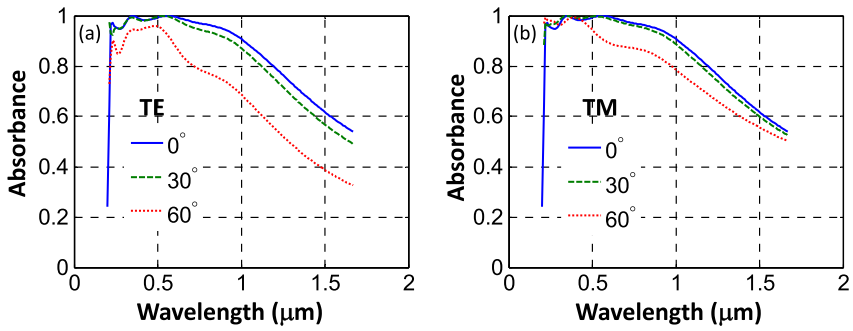

Fig. 6. Angular absorbance for the visible (VIS) wavelength metamaterial perfect absorber in Fig. 4(a). $t_{Ti} = 4.1$ nm, $t_{Ni} = 13$ nm, and $t_{Al} = 54$ nm. $t_{DS1} = t_{DS2} = t_{DS3} = 50$ nm. (a) TE polarized light. (b) TM polarized light.

Fig. 4(a). The broadband absorption does not degrade significantly with incident angle. The physical reason is that the field penetration through the metallic thin films in a multi-junction configuration is not affected dramatically by the oblique incidence. Essentially, the optical path length inside the metallic films becomes longer for larger incidence angles, and this is the reason for the slight degradation in broadband absorption. The optical path length in the dielectric layers also becomes longer for oblique incidence, but the geometrical tolerance in dielectric thickness is, in general, greater than the tolerance for the metallic film thickness, in the case of our multi-junction thin-metal based design. It is also worth mentioning that TM polarization has a better angular response than TE polarization. This is due to the fact that the reflectance at the metal-dielectric interface can increase more pronouncedly for TE polarization. The in-plane electric field intensity in TM polarization can facilitate the transmission at a hetero-material interface.

In addition to the film thin field penetration-absorption and the sequential arrangement in the material $n - k$ for the multi-junction configurations the cancelation of the reflected wave is a critical consideration for a high absorption. Since the transmittance vanishes for the current structure due to the high-extinction bottom aluminum layer, a lowered reflectance directly contributes in a high absorbance. In the case of a planar structure without grating couplers, the most important consideration for a light trapped device is so-called impedance matching. The wave impedance is defined as the total electric field intensity over the total magnetic field intensity at a specific location

$$Z(\vec{r}) = \frac{E_i(\vec{r}) + E_r(\vec{r})}{H_i(\vec{r}) + H_r(\vec{r})} \tag{1}$$

where E and H are the electric and magnetic field intensity, and subscript i and r represent the incident and reflected waves. In order to achieve a fully matched wave impedance condition at the air-multilayer interface, the wave impedance seen by the incident photons at the multi-layer stack should be as close to the air as possible. This certainly reduces the total reflection at the air-device interface at harmonic steady state and results in a very high absorption. In fact, the multi-junction concepts and the impedance matching have not been carefully examined in the case of metamaterial perfect absorbers (MPA), based on our literature review. Fig. 7 plots the wave impedance seen by the incident photons at $z_0 = 1$ μm above device top surface with a parametric sweeping to form a trace. $z_0 = 1$ μm is chosen because it corresponds to the simulation domain top boundary. In fact, the wave impedance value (Z) at any z-cut above the MPA will give the same result. The polar plots in a complex plane are the most versatile and obvious way to observe the wave impedance variation with the parameters. Fig. 7(a) plots Z versus $t_{SiO2} = t_{DS1} = t_{DS2} = t_{DS3}$, Fig. 7(b) plots Z versus t_{Ti}, and Fig. 7(c)

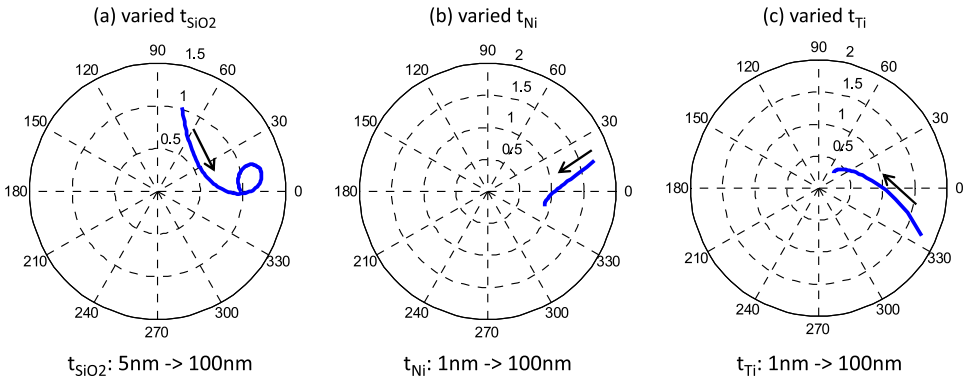

Fig. 7. Wave impedance (Z) seen by the incident photons at $z_0 = 1$ μm above device top surface, which corresponds to the simulation domain top boundary, for varied layer thicknesses. The perfect impedance matched condition is $1 + 0i$. (a) Silicon dioxide thickness ($t_{DS1} = t_{DS2} = t_{DS3} = t_{SiO2}$) varies from 5 nm to 100 nm. The other dimensions are $t_{Ti} = 4.1$ nm, $t_{Ni} = 13$ nm, and $t_{Al} = 54$ nm. (b) Ni thickness (t_{Ni}) varies from 1 nm to 100 nm. The other dimensions are $t_{Ti} = 4.1$ nm, $t_{Al} = 54$ nm, and $t_{Ds1} = t_{DS2} = t_{DS3} = 50$ nm. (c) Ti thickness (t_{Ti}) varies from 1 nm to 100 nm. The other dimensions are $t_{Ni} = 13$ nm, $t_{Al} = 54$ nm, and $t_{Ds1} = t_{DS2} = t_{DS3} = 50$ nm. The geometrical parameter selection is from Fig. 4(a).

plots Z versus t_{Ni}. For Fig. 7(a), it is observed that for a thin SiO_2 layer thickness, the wave impedance can deviate from air, i.e. $1 + 0i$, significantly. This is due to the multiple metallic layers become too closely spaced, and the interference conditions for a low reflectance cannot be achieved. For the extreme case of three metal layers being directly stacked on each other, the bulk metallic property will be seen instead of thin-film interference. For a thicker SiO_2 layer > 50 nm, the impedance matching condition can be preserved. This is because further apart ultra-thin metallic films facilitate the field penetration. Certainly, the thinnest possible thickness that can still preserve field penetration is the most desirable, in order to minimize the device thickness. For the metallic layer thickness, parameter sweeping is shown in Fig. 7(b) and (c). The problem associated with the thick metal film is self-evident since the field penetration is absent. In this case, significant field reflection amplitude exists, and this degrades the total wave impedance from $1 + 0i$, at the air-device interface. For an excessively thin metallic layer thickness, the insufficient wave absorption leads to the photons can be reflected by the bottom thick Al layer and afterward leave the material stacks. This results in non-negligible reflection and degrades Z value from $1 + 0i$.

4. Experimental Results for SiO_2/Ti/ SiO_2/Ni/SiO_2/Al Compact Metamaterial Perfect Absorbers

The experiment is conducted using an AST PEVA 600I multi-target electron gun (e-gun) evaporator. The measurement of the absorption spectrum of the sample is conducted using a Hitachi U-4100 ultraviolet-visible-near-infrared (UV-VIS-NIR) spectrometer over the wavelength range from 300 nm to 2600 nm. Although the planar structure, in general, only results in specular reflection and transmission, i.e. zeroth order reflection and transmission, an integration sphere is still used to measure the total reflectance and the total transmittance. Due to the multiple dielectric-metal layered structure, the transmittance is zero over the entire spectral range. The bared silicon wafer is cleaned first using standard RCA clean process. Afterward, a 54 nm aluminum (Al) is deposited on the wafer. Subsequently, a 50 nm silicon dioxide (SiO_2), 13 nm nickel (Ni), 50 nm silicon dioxide (SiO_2), and 4.1 nm titanium (Ti), and 50 nm silicon dioxide (SiO_2) are deposited successively. It should be noted that the deposition of the ultra-thin Al, Ni, Ti metallic film using e-gun evaporator is a low-cost method and fully compatible with silicon photonics. The measured spectral response is shown in Fig. 8. Since

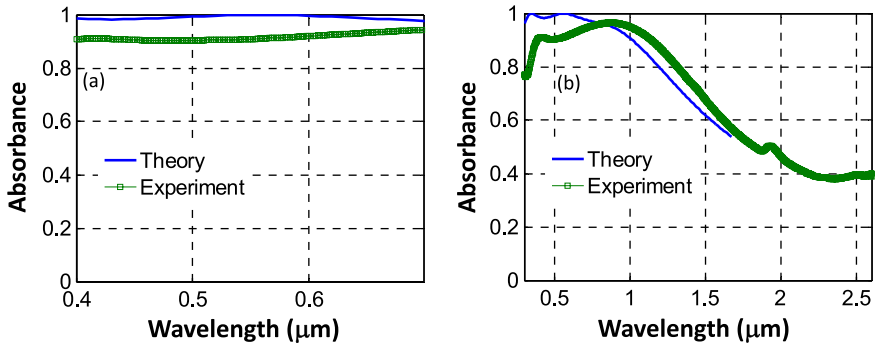

Fig. 8. Measured spectral absorbance for multi-metal MPA consisting of Ti, Ni, and Al multi-junctions. This is for the metamaterial perfect absorber at visible wavelength range, corresponding to Fig. 4(a). The dimensions are $t_{Ti} = 4.1$ nm, $t_{Ni} = 13$ nm, $t_{Al} = 54$ nm, and $t_{Ds1} = t_{DS2} = t_{DS3} = 50$ nm. (a) The zoom-in of the spectral response from $\lambda = 0.4$ μm to 0.7 μm. (b) Full spectral response from $\lambda = 0.3$ μm to 2.6 μm.

the transmittance is zero over the entire wavelength range of interest, the absorbance is one minus the reflectance. To focus on the metamaterial perfect absorber performance at visible wavelength range, we particularly show the data from $\lambda = 400$ nm to $\lambda = 700$ nm in the left of Fig. 8, which corresponds to the visible light and is the wavelength range employed in our genetic algorithm optimization. The slight discrepancy between the experiment and the theoretical value is due to the thin-film thickness control and the surface morphology. Due to the very thin thickness in e-gun deposition, the control of the thickness takes some experience to adjust it to a correct value. As a result, the experimental value for the absorbance can be further improved if the process condition can be better handled with iterative trials. For the surface morphology issues, the e-gun films inevitably have certain roughness in the range of 1 nm RMS roughness value. For a fully planar smooth film, atomic layer deposition (ALD), molecular beam epitaxy (MBE), or metalorganic chemical vapor deposition (MOCVD) can be used, although the cost can be higher.

5. Conclusion

In this work, we proposed a fully planarized, compact metamaterial perfect absorber, using a multi-metal configuration. The theoretical values of unity absorption can be achieved while the device thickness in our proposed design is only 221 nm for the visible wavelength range, comparable to the silver plasmonics-based metamaterial perfect absorber at the same wavelength range [9]. The wavelength scalability is demonstrated using adjusted film thickness, and it is shown that the multi-junction design can be scaled to different wavelength ranges. The planar nature of the design eliminates the need for lithography and etching, which facilitates scaling for large-area photonic applications. The physics is explained using optical field penetration-absorption at the thin-film metallic layers. Additionally, the correct selection of the metallic materials and the arrangement of their $n - k$ values in the spectrum are the key parts for realizing such a multi-junction multiple-metal configuration. The wave impedance matching with parametric sweeping in different layer thicknesses is further utilized to analyze the underlying physics and design constraints. It is clear that a properly optimized film thickness using GA is important to have a fully matched impedance to air, as far as the incident photons are concerned. The initial experimental result is provided for our newly proposed metamaterial perfect absorber, and a closely matched and firmly supported measured spectral absorption is observed, compared to the theoretical result. An even closer-to-unity absorption can surely be achieved experimentally if the thin-film thickness control and the morphology are adjusted in a more elaborate manner.

References

[1] C. M. Watts, X. Liu, and W. J. Padilla, "Metamaterial electromagnetic wave absorbers," *Adv. Opt. Mater.*, vol. 24, no. 23, pp. OP98–OP120, Jun. 2012.
[2] W. H. Emerson, "Electromagnetic wave absorbers and anechoic chambers through the years," *IEEE Trans. Antennas. Propag.*, vol. AP-21, no. 7, pp. 484–490, Jul. 1973.
[3] N. Liu, M. Mesch, T. Weiss, M. Hentschel, and H. Giessen, "Infrared perfect absorber and its application as plasmonic sensor," *Nano Lett.*, vol. 10, no. 7, pp. 2342–2348, Jul. 2010.
[4] D. Dregely *et al.*, "3D optical Yagi-Uda nanoantenna array," *Nat. Commun.*, vol. 2, no. 94, p. 267, Apr. 2010.
[5] D. Schurig*et al.*, "Metamaterial electromagnetic cloak at microwave frequencies," *Science*, vol. 314, no. 5801, pp. 977–980, Nov. 2008.
[6] B. A. Munk, *Frequency Selective Surfaces: Theory and Design*. New York, NY, USA: Wiley, 2000.
[7] X. Liu *et al.*, "Taming the blackbody with infrared metamaterials as selective thermal emitters," *Phys. Rev. Lett.*, vol. 107, no. 4, Jul. 2011, Art. no. 045901.
[8] C. Wu *et al.*, "Metamaterial-based integrated plasmonic absorber/emitter for solar thermo-photovoltaic systems," *J. Opt.*, vol. 14, no. 2, Jan. 2012, Art. no. 024005.
[9] K. Aydin, V. E. Ferry, R. M. Briggs, and H. A. Atwater, "Broadband polarization-independent resonant light absorption using ultrathin plasmonic super absorbers," *Nat. Commun.*, vol. 2, no. 10, p. 517, Nov. 2011.
[10] Y. Avitzour, Y. A. Urzhumov, and G. Shvets, "Wide-angle infrared absorber based on a negative-index plasmonic metamaterial," *Phys. Rev. B, Condens. Matter Mater. Phys.*, vol. 79, no. 4, Jan. 2008, Art. no. 045131.
[11] J. Hao *et al.*, "High performance optical absorber based on a plasmonic metamaterial," *Appl. Phys. Lett.*, vol. 96, no. 25, Jun. 2010, Art. no. 251104.
[12] H. Tao *et al.*, "A dual band terahertz metamaterial absorber," *J. Phys. D, Appl. Phys.*, vol. 43, no. 22, May 2010, Art. no. 225102.
[13] H. Tao *et al.*, "A metamaterial absorber for the terahertz regime: Design, fabrication and characterization," *Opt. Exp.*, vol. 16, no. 10, pp. 7181–7188, May 2008.
[14] H. Tao *et al.*, "Highly flexible wide angle of incidence terahertz metamaterial absorber: Design, fabrication, and characterization," *Phys. Rev. B, Condens. Matter Mater. Phys.*, vol. 78, no. 24, Dec. 2008, Art. no. 241103.
[15] D. Ji *et al.*, "Broadband absorption engineering of hyperbolic metafilm patterns," *Sci. Rep.*, vol. 4, p. 4498, 2014.
[16] Y. Cui *et al.*, "Ultrabroadband light absorption by a sawtooth anisotropic metamaterial slab," *Nano Lett.*, vol. 12, no. 3, pp. 1443–1447, Mar. 2012.
[17] C. Argyropoulos, K. Q. Le, N. Mattiucci, G. D'Aguanno, and A. Alu, "Broadband absorbers and selective emitters based on plasmonic Brewster metasurfaces," *Phys. Rev. B, Condens. Matter Mater. Phys.*, vol. 87, no. 20, May 2013, Art. no. 205112.
[18] *Rsoft CAD User Manual*, 8.2 ed. Rsoft Design Group, New York, NY, USA, 2010.
[19] Y. K. Zhong, S. M. Fu, N. P. Ju, P. Y. Chen, and A. Lin, "Experimentally-implemented genetic algorithm (Exp-GA): toward fully optimal photovoltaics," *Opt. Exp.*, vol. 23, no. 19, pp. A1324–A1333, Sep. 2015.
[20] Y.-J. Chang and Y.-T. Chen, "Broadband omnidirectional antireflection coatings for metal-backed solar cells optimized using simulated annealing algorithm incorporated with solar spectrum," *Opt. Exp.*, vol. 19, no. S4, pp. A875–A887, Jul. 2011.
[21] A. Lin and J. D. Phillips, "Optimization of random diffraction gratings in thin-film solar cells using genetic algorithms," *Sol. Energ. Mater. Sol.*, vol. 92, no. 12, pp. 1689–1696, Dec. 2008.
[22] D. E. Goldberg, *Genetic Algorithms in Search, Optimization, and Machine Learning*, 1 ed. Reading, MA, USA: Addison-Wesley, 1989.
[23] A. E. Eiben and J. E. Smith, *Introduction to Evolutionary Computing*. Berlin, Germany: Springer-Verlag, 2008.
[24] S. Preblea, M. Lipson, and H. Lipson, "Two-dimensional photonic crystals designed by evolutionary algorithms," *Appl. Phys. Lett.*, vol. 86, no. 6, Feb. 2005, Art. no. 061111.
[25] L. Shen, Z. Ye, and S. He, "Design of two-dimensional photonic crystals with large absolute band gaps using a genetic algorithm," *Phys. Rev. B, Condens. Matter Mater. Phys.*, vol. 68, no. 3, Jul. 2003, Art. no. 035109.
[26] A. D. Rakić, A. B. Djurišic, J. M. Elazar, and M. L. Majewski, "Optical properties of metallic films for vertical-cavity optoelectronic devices," *Appl. Opt.*, vol. 37, no. 22, pp. 5271–5283, Aug. 1998.